Image-guided surgery with a new tumour-targeting probe improves the identification of positive margins

Masahide Goto,[a] Ingeun Ryoo,[a] Samer Naffouje,[a,b] Sunam Mander,[a] Konstantin Christov,[a] Jing Wang,[c] Albert Green,[a] Anne Shilkaitis,[a] Tapas K. Das Gupta,[a] and Tohru Yamada[a,d]*

[a]Department of Surgery, Division of Surgical Oncology, University of Illinois College of Medicine, Chicago, IL 60612, USA
[b]Surgical Oncology, Moffitt Cancer Center, Tampa, FL 33612, USA
[c]Department of Mathematics, Statistics and Computer Science, University of Illinois College of Liberal Arts and Sciences, IL 60607, USA
[d]Department of Bioengineering, University of Illinois College of Engineering, Chicago, IL 60607, USA

eBioMedicine 2022;76: 103850
Published online xxx
https://doi.org/10.1016/j.ebiom.2022.103850

Summary

Background Given the lack of visual discrepancy between malignant and surrounding normal tissue, current breast conserving surgery (BCS) is associated with a high re-excision rate. Due to the increasing cases of BCS, a novel method of complete tumour removal at the initial surgical resection is critically needed in the operating room to help optimize the surgical procedure and to confirm tumour-free edges.

Methods We developed a unique near-infrared (NIR) fluorescence imaging probe, ICG-p28, composed of the clinically nontoxic tumour-targeting peptide p28 and the FDA-approved NIR dye indocyanine green (ICG). ICG-p28 was characterized *in vitro* and evaluated in multiple breast cancer animal models with appropriate control probes. Our experimental approach with multiple-validations and -blinded procedures was designed to determine whether ICG-p28 can accurately identify tumour margins in mimicked intraoperative settings.

Findings The *in vivo* kinetics were analysed to optimize settings for potential clinical use. Xenograft tumours stably expressing iRFP as a tumour marker showed significant colocalization with ICG-p28, but not ICG alone. Image-guided surgery with ICG-p28 showed an over 6.6×10^3-fold reduction in residual normalized tumour DNA at the margin site relative to control approaches (i.e., surgery with ICG or palpation/visible inspection alone), resulting in an improved tumour recurrence rate (92% specificity) in multiple breast cancer animal models independent of the receptor expression status. ICG-p28 allowed accurate identification of tumour cells in the margin to increase the complete resection rate.

Interpretation Our simple and cost-effective approach has translational potential and offers a new surgical procedure that enables surgeons to intraoperatively identify tumour margins in a real-time, 3D fashion and that notably improves overall outcomes by reducing re-excision rates.

Funding This work was supported by NIH/ National Institute of Biomedical Imaging and Bioengineering, R01EB023924.

Keywords: Real-time imaging; Cell-penetrating peptide; Near-infrared fluorescence; Tumour margin

Introduction

Breast cancer is primarily treated via surgical excision of the tumour with the surrounding normal breast tissue margin. In the early stage, these treatments take the form of breast-conserving surgery (BCS) or lumpectomy.[1] Although BCS provides satisfactory cosmetic outcomes, the re-resection rate is ~20%, and of these surgeries, ~85% are performed due to the presence of initial positive margins.[2] Although there is often a need for further surgery and additional tissue removal owing to the inherent challenges in achieving negative margins, existing guidelines recommend against excising a wider negative margin in routine practice.[3] Currently, surgeons rely primarily on visual and tactile cues to distinguish between healthy and malignant tissues

*Corresponding author at: Department of Surgery, Division of Surgical Oncology, University of Illinois College of Medicine, Chicago, IL 60612, USA.
E-mail address: tohru@uic.edu (T. Yamada).

Research in context

Evidence before this study

The positive margin rate following breast-conserving surgery (lumpectomy) is unignorably high. Although current methods of tumour margin assessment such as frozen section, imprint cytology, and intraoperative ultrasound are helpful, there is a clinical need for simple and accurate methods to intraoperatively identify tumour margins. NIR imaging is a promising approach and ICG as an NIR contrast agent has been tested in translational and clinical studies. ICG is a bright NIR dye and has an excellent safety record in humans. However, it is likely that the lack of ligand specific binding allows it to easily leak out of the tumour. To overcome the limitations of ICG is to utilize tumour-targeted molecules labelled with ICG. With a similar approach, several other NIR imaging agents are currently under investigation, although few are approved for clinical use.

Add value of this study

In this study, we established a new near-infrared fluorescence imaging probe ICG-p28 by utilizing ICG labeled with the cell-penetrating peptide carrying a tumour-targeting motif. This study demonstrated that intraoperative imaging with ICG-p28 accurately identified the tumour margins, improving tumour recurrence rate in multiple breast cancer animal models independent of the receptor expression status.

Implications of all the evidence available

Based on results obtained from clinically relevant studies, this paper highlights the significance of our imaging approach and translational potential. The simple and cost-effective real-time imaging with ICG-p28 can offer a positive impact on surgical treatment outcomes.

and thus may leave residual lesions in the tumour bed.[4] MRI, mammography, ultrasound, and CT etc. are readily available imaging modalities typically used to assess the tumour lesion prior to the surgical procedure. Although these traditional imaging modalities have been of immense help in advancing tumour detection and determining the extent of resection(s),[5] the need for accurate intraoperative imaging remains one of the most important unmet needs in the management of breast cancer at the time of the initial BCS.

Extensive research is ongoing to identify new, rapid, and accurate intraoperative margin assessment tools, some of which are currently undergoing clinical testing.[6] For example, among biophotonic-based techniques, image-guided surgery using fluorescence imaging offers many advantages for surgeons. Near-infrared (NIR) imaging is an emerging biomedical imaging modality for fluorescence-guided surgery because of its significant light absorption, ability to assist in real-time visualization, and lack of ionizing radiation. *In vivo* imaging in the NIR range (700−900 nm) is superior to that in the visible spectrum owing to its low scattering, negligible tissue autofluorescence, and relatively high tissue penetration.[7] The first FDA-approved NIR dye, indocyanine green (ICG), has been used in clinical practice to determine the liver function, cardiac output, and blood flow etc) for over fifty years due to its proven safety and the feasibility of its use. Also, ICG has been tested for tumour margin identification.[8–10] Although ICG can localize to breast tumours, the primary disadvantages of ICG are its short half-life, and its lack of a tumour-specific interaction mechanism as a passive fluorescent dye.[9,11,12] Thus, creating a new tumour-targeted version of ICG could overcome the limitations and be more useful in the clinic.

The tumour-targeted delivery of imaging agents or drugs is one of the major challenges in cancer therapy.[13] As targeted delivery could improve the usefulness of such agents, various delivery vehicles, including small molecules, antibodies, proteins, and peptides, have been investigated.[14] Peptides are generally more specific than small molecules due to their high complexity and are relatively inexpensive to manufacture. In particular, cell-penetrating peptides (CPPs) have been shown to be a promising agent for improving the delivery and intracellular uptake of diagnostic and therapeutic agents.[15] They also have advantages over greater molecular weight antibodies in terms of feasibility of synthesis, derivatization flexibility, low immunogenicity, and physicochemical parameters.[16] These characteristics suggest that the development of CPPs as carrier molecules is a promising strategy for tumour-targeted delivery.

We previously reported that *Pseudomonas aeruginosa* azurin and its derived peptide p28 preferentially enter various cancer cells[17] and induce antiproliferative effects.[18,19] As a single therapeutic agent, p28 (NSC745104) was tested in two phase I clinical trials and granted the FDA Orphan Drug and Rare Pediatric Disease designations due to its demonstrated preliminary efficacy without apparent adverse effects, toxicity or immunogenicity in patients with advanced solid tumours and in paediatric patients with recurrent and refractory central nervous system tumours (NCI and Pediatric Brain Tumor Consortium).[20–22] As such, p28 is a potentially ideal CPP that can serve as a tumour-targeted carrier[17,18,21,22] since it preferentially penetrates cancer cells,[17,18] is highly water soluble and stable,[23] and clinically exhibits no significant adverse effects, toxicity or immunogenicity in humans.[21,22] Here, we developed a new noninvasive NIR-based probe, ICG-p28, composed of clinically nontoxic p28 and FDA-approved ICG. Our approach was not designed for tumour diagnosis (tumour localization). Our experiments were specifically designed to improve the identification of positive margins, intraoperatively. We report that

image-guided surgery with ICG-p28 clearly defines margins in a real-time, 3D fashion, resulting in adequate tumour excision in clinically relevant settings. These findings hold promise for improved outcomes in BCS and can guide the development of simplified (in terms of overall procedure/operation time)[24] and more cost-effective protocols.

Methods

Peptide synthesis and ICG conjugation

Peptides, p28, retro-inverso p28 (RI p28), and AA3H[25] were synthesized by CS Bio, Inc. at >95% purity and mass balance. Peptides were dissolved in PBS buffer at pH 7 and reacted with ICG-maleimide in anhydrous DMSO for 3 h at room temperature in the dark.[26] The reactions were dialyzed (M.W. 2000 cut-off, Pierce) against PBS at 4 °C for 24 h and purified by filtration over Sephadex G-25 (GE Healthcare). The final products were identified by HPLC and MALDI mass spectroscopy.

ICG-p28 characterization

The PDE neo® (Photodynamic Eye; Mitaka USA, UT) is an FDA 510(k)-cleared NIR camera composed of a charge-coupled device (CCD) camera unit that detects an 800 nm NIR signal. In general, the PDE unit (camera connected to a small control unit and LCD monitor) has been used for NIR imaging clinical applications with ICG for identifying hepatic segments and bile ducts.[27] ICG and ICG-p28 in 20% intralipid emulsion (Sigma; St. Louis, MO), which reportedly mimics the light scattering and absorption properties of tissue,[28] were recorded by the PDE camera unit. Various concentrations of ICG-p28 (0.2 pM to 20 μM) and ICG were monitored at 3 mW/cm² excitation.

Construction of breast tissue-mimicking phantoms

Optical technology at the NIR wavelength for tissue measurement is advantageous because it can avoid the influence of autofluorescence and allow measurements of relatively deep tissues. To determine the depth detection limit, tumour-simulating inclusions containing ICG-p28 were incorporated into tissue phantoms at predefined locations and imaged with the PDE unit. A previously published procedure for making tissue phantoms[29,30] was followed with modifications, as illustrated in *Supplemental Figure S1*. Briefly, 10% gelatine powder (Spectrum; New Brunswick, NJ) was dissolved in 50 mM Tris buffer containing 150 mM NaCl at pH 7.4. The gelatine was dissolved by stirring at 50 °C, followed by cooling to 37 °C. Bovine haemoglobin and intralipid (20%; Sigma) were then added. To determine the maximal penetration depth of the NIR fluorescence signal, an inclusion containing 200 nM ICG-p28 was positioned in the phantom tissue. Subsequently, the phantom tissue was excised in 2 mm layers at a time towards the inclusion. At all depths, real-time imaging was performed with an intraoperative PDE neo system. The distance between the PDE camera and the phantom was fixed at 200 mm. The intensity of the images acquired using the PDE neo system was rated quantitatively. The mean±SD values were calculated.

Cell cultures

The human breast cancer cell lines MDA-MB-231 (ATCC Cat#: HTB-26, RRID: CVCL_0062) and IOWA-1T (ATCC Cat# CRL-3292, RRID:CVCL_6G16) were obtained from American Type Culture Collection (Manassas, VA). MDA-MB-231-iRFP cells were established and characterized in our laboratory. MDA-MB-231 cells were transfected with the piRFP plasmid with Lipofectamine 2000 (Invitrogen). Transfectants stably expressing the iRFP gene were selected in the presence of puromycin at 0.5 μg/ml. They were cultured in MEME medium supplemented with 10% heat-inactivated foetal bovine serum at 37 °C in a humidified incubator with 5% CO_2. Single-generation patient-derived xenograft (PDX) cells of triple-negative breast cancer cells (Model ID: TM00090) were obtained from Jackson Laboratory.

Detection of cancer cells *in vitro* by ICG-p28

MDA-MB-231 cells were treated with 0.5 mg/kg (~130 nM) ICG-p28 followed by 2 h incubation at 37 °C in a humidified incubator with 5% CO_2. Cells were then washed with PBS, trypsinized and counted. Various cell numbers at 100,200,300, and 500 per 1 μl volume (=1 mm diameter) were imaged with the PDE unit.

Animal models

Tumour models were established by subcutaneously (*s.c.*) implanting 1.0×10^6 MDA-MB-231, IOWA-1T or MDA-MB-231-iRFP cells into the right back (kinetic analysis) and mammary fat pads (MFPs; qualitative margin analysis) of 4- to 5-week-old female athymic mice (Jackson Laboratory). For additional quantitative margin analysis, tumour models were established by implanting triple-negative PDX cells (stage IV) in the MFPs of 4- to 5-week-old female NOD/Scid/IL2Rγ^{null} (NSG) mice (Jackson Laboratory). The animal surgeon was blinded to the experimental conditions such as animal identification and treatment group.

In vivo kinetic analysis of ICG-p28

MDA-MB-231 cells were injected *s.c.* into 4- to 5-week-old female athymic mice. ICG-p28 or ICG alone was injected intravenously (*i.v.*) (tail vein) at 0.2, 0.5, or 1 mg/kg-b.w. Animals were imaged using an Odyssey scanner (LI-COR Biosciences) at 6–72 h post *i.v.*

administration. The tumour background ratio (TBR) was determined using ImageJ software (National Institutes of Health), where a region of interest (ROI) was drawn over the whole tumour and a background ROI was drawn over adjacent tissue. An ROI was manually generated around each tumour (800 nm channel).

Tumour margin assessment

MDA-MB-231-iRFP cells (1.0×10^6 cells in 0.1 ml PBS) were inoculated *s.c.* into the right back of mice. Athymic mice bearing tumours received *i.v.* ICG-p28 or ICG at 0.5 mg/kg-b.w. Twenty-four hours after injection, whole tumours (~200 mm^3) in each group were resected along with surrounding tissue. Specimens were imaged *ex vivo* with an Odyssey scanner with the 700 nm channel for iRFP and the 800 nm channel for ICG-p28 or ICG alone. The area measurements were determined by ImageJ, and concordance rates of fluorescent signals from 700 and 800 nm in each group [ICG-p28 group (n = 10) and ICG alone group (n = 5)] were calculated. The mean+SD values were calculated.

Quantitative assessment of ICG-p28 for tumour margin determination and tumour recurrence follow-up

Once NSG mice developed PDX tumours of similar sizes (200–300 mm^3), the mice were randomly divided into five groups: ICG-p28, ICG alone, ICG-AA3H peptide, ICG-RI p28, and PBS. Each agent was injected *i.v.* (tail vein) with the corresponding compound at the equivalent of ICG-p28 0.5 mg/kg-b.w. Twenty-four hours after injection, all surgical procedures were started under sterile conditions. Following anaesthesia administration, the PDE imaging system was used to monitor NIR fluorescence throughout the entire surgical procedure. For the PBS group, malignant tissue identified via visual and tactile cues was resected under white-light illumination, while only tissue demonstrating contrast enhancement was resected in the ICG, ICG-p28, ICG-AA3H, and ICG-RI p28 groups; images of the fluorescence signal were displayed on an adjacent monitor, and all ICG-positive tissue foci (suspected as tumour tissues) were excised. For all groups, whole tumour removal (200–300 mm^3) with an approximately 2 mm safety margin was performed under guidance of the PDE imaging system (except the PBS control group). The remaining surgical bed/surrounding mammary tissue at the 6 and 12 o'clock positions was also resected with approximately 2 mm in contiguous dimensions (~2 mm^3 in each sample and group). Following tumour excision, the skin incisions were closed using a nylon suture, and the mice were returned to their cages and kept for an additional four weeks and monitored for tumour recurrence. Four weeks after surgery, the mice were evaluated to determine whether any of the tumours had recurred due to remnant positive margins at the resection site.

Detection of residual cancer cells in the tumour margin by Alu sequencing

A quantitative analysis using human-specific Alu sequence (huAlu) was performed on samples collected from the margins. Since Alu-repeat DNA sequences are specific to human cells,[31] human-derived tumours implanted into mice can be identified by detecting the presence of huAlu. We standardized the quantitative detection of huAlu in resected tumours and surrounding margin tissues according to previously published methods.[32,33] Human tumour cells in the five groups (ICG-p28, ICG alone, ICG-AA3H, ICG-RI p28, and PBS; 8 mice in each group) were identified based on the quantitative detection of huAlu present in the mice. Genomic DNA was extracted from harvested tissues using the DNeasy Blood & Tissue Kit (Qiagen). To identify human cells in the mouse tissues, primers specific for huAlu (sense: 5′- ACG CCT GTA ATC CCA GCA CTT -3′; and antisense: 5′- TCG CCC AGG CTG GAG TGC A -3′) were used to amplify the huAlu repeats present in the extracted genomic DNA by real-time PCR (5 ng genomic DNA, 0.5 µM each primer, and PowerUp SYBR Green Master Mix; Life Technologies, USA). Each reaction was performed in a final volume of 10 µl under the following conditions: polymerase activation at 50 °C for 2 min and 95 °C for 2 min followed by 30 cycles at 95 °C for 30 sec, 63 °C for 30 sec, and 72 °C for 30 sec. A quantitative measure of amplifiable mouse DNA was obtained through amplification of the mouse GAPDH genomic DNA sequence (mGAPDH) with mGAPDH-specific primers (sense: 5′- AGG TCG GTG TGA ACG GAT TTG -3′; antisense: 5′- GGG GTC GTT GAT GGC AAC A -3′) using the same PCR conditions described for huAlu. The fluorescence emitted by the reporter dye was detected, and the threshold cycle (Ct) was recorded as a quantitative measure of the amount of PCR product in each sample. The amount of huAlu DNA and mGAPDH DNA in the margins was calculated by comparison with a standard curve, and the calculated amount of huAlu DNA was normalized against the relative quantity of mGAPDH. The mean±SD values were calculated.

Histological analysis

Resected tissues were placed in containers prefilled with buffered 3.7% formalin (Anatech) and fixed for 24 h. Formalin was replaced with 70% ethanol following fixation. Samples were paraffin-embedded, and blocks were cut into 4 μm-thick sections and mounted onto slides. Ki-67 (Lab Vision Cat# RM-9106, RRID:AB_2,341,197)- and H&E-stained slides were analysed by a pathologist blinded to the experimental groups and surgical

resection results. The pathologist was responsible for determining a tumour's presence, margin status, and general characteristics of resected tissues.

Ethics statement

All experiments were approved by University of Illinois at Chicago (UIC) Institutional Animal Care and Use Committee (IACUC) and conformed to the guidelines set by United States Animal Welfare Act and the National Institutes of Health.

Statistical analysis

To achieve robust and unbiased results, our study included the use of appropriate statistical methods, prospective sample size/replications, and standards (negative- and positive-controls) in addition to blinded procedure during experiments. Animal models proposed in this application included randomization and multiple experimental models to maintain scientific integrity and reproducibility. Power analysis was done to determine appropriate animal size for the studies. The effect size (F) was calculated from the squared difference among means of ratio (tumour/normal tissue) of fluorescence intensities that is anticipated or desired, divided by the maximum variance. Power was then calculated by using the function pwr.anova.test in R package pwr. The minimum number of animal/group (Sample size) was estimated, suggesting that the sample group size 8 was sufficient to run the experiment. Data processing and statistical analysis were performed using GraphPad Prism ver. 8 (GraphPad Software) and R version 4.0.5 (The R Foundation for Statistical Computing). Friedman's nonparametric rank test was used for recurrent tumour volume data. F test was used for Alu sequences after validating the normality for its log transformation as shown in *Supplementary Figure S5*. Two-sided testing was performed for each analysis, and $P < 0.05$ was considered statistically significant.

Role of the funding source

Funding source had no role in the study design, data collection, data analyses, data interpretation, writing of the report and the decision to submit the manuscript for publication.

Results

ICG-p28 characterization *in vitro* and kinetics *in vivo*

Because ICG-p28 is a new NIR compound whose properties have yet to be explored, we characterized its photochemical properties with a PDE neo® imaging unit, an FDA 510(k)-cleared NIR system composed of a CCD camera unit that detects 800 nm NIR signals. This PDE system (the camera coupled with a small control unit and an LCD monitor) has been used for clinical applications involving NIR imaging with ICG for identifying hepatic segments and bile ducts, among other physiological systems.[34,35] The advantage of the PDE unit lies in its size and portability, which enables surgeons to hold the camera unit (1.1 lb) and easily obtain real-time NIR images from various angles during surgery. First, we tested the sensitivity of the PDE unit in detecting ICG-p28. ICG-p28 was placed in a 5% intralipid emulsion, which reportedly mimics the light scattering and absorption properties of tissue.[36] Both ICG-p28 and ICG alone showed almost identical fluorescence quantum yields (ΦFs) at concentrations ranging from 0.2 pM to 20 μM in a concentration-dependent manner (Figure 1a). The use of antibodies conjugated to ICG is limited, as ICG loses its NIR fluorescence due to the interaction between ICG and IgG molecules with large molecular weights/multiple domains (~150 kDa).[37] In contrast, when ICG was conjugated to p28, it did not lose its fluorescence, probably due to the size of p28 (2.9 kDa, ~1/50 the size of IgG).

The results of preclinical[23] and two phase I clinical trials of p28 as a monotherapeutic agent[21,22] have identified the therapeutic dose of p28 for treating cancer patients. Since fluorescent imaging techniques rely on the concentration of each contrast agent,[38] the optimum dose range for ICG-p28 in mice with MDA-MB-231 human breast cancer tumours was determined with the PDE unit. Each mouse was injected *i.v.* with ICG-p28 or ICG alone at 0.2–1.0 mg/kg (~50 to 250 nM). The mice were imaged at various time points (6–72 h), and the ratio of the NIR signal intensity of the tumour tissue and normal tissue (thigh) was calculated. Significant contrast between the tumour and surrounding normal tissues was detected at 24 h following the injection of ICG-p28 at 0.2–1.0 mg/kg (Figure 1b). As the higher doses of ICG-p28 (>1.0 mg/kg) required a longer time to achieve clear contrast ("washout") because of the high background signal, the tumour-specific signal was determined to be optimal at 0.2–0.5 mg/kg concentrations within a practical time scale (24 h) for clinical use (Figure 1b). In contrast, ICG alone at the same dose was excreted rapidly, and the tumour site could not be distinguished (tumour/normal tissue ratio ~1) according to the NIR images (Figure 1b). This result illustrates the preferential uptake of p28, which leads to longer retention at the tumour site and clear contrast imaging of the tumour vs. surrounding tissue.

As described earlier, the use of optical technology at the NIR wavelength for tissue measurement is advantageous, as it can avoid the influence of autofluorescence and allow measurements of relatively deep tissues.[39] To determine the detection limit of the objective size and depth, various sizes of tumour-simulating inclusions containing ICG-p28 (Figure 1c) and phantoms[40] incorporating these inclusions at predefined locations (Figure 1d) were imaged with the PDE unit. Even with

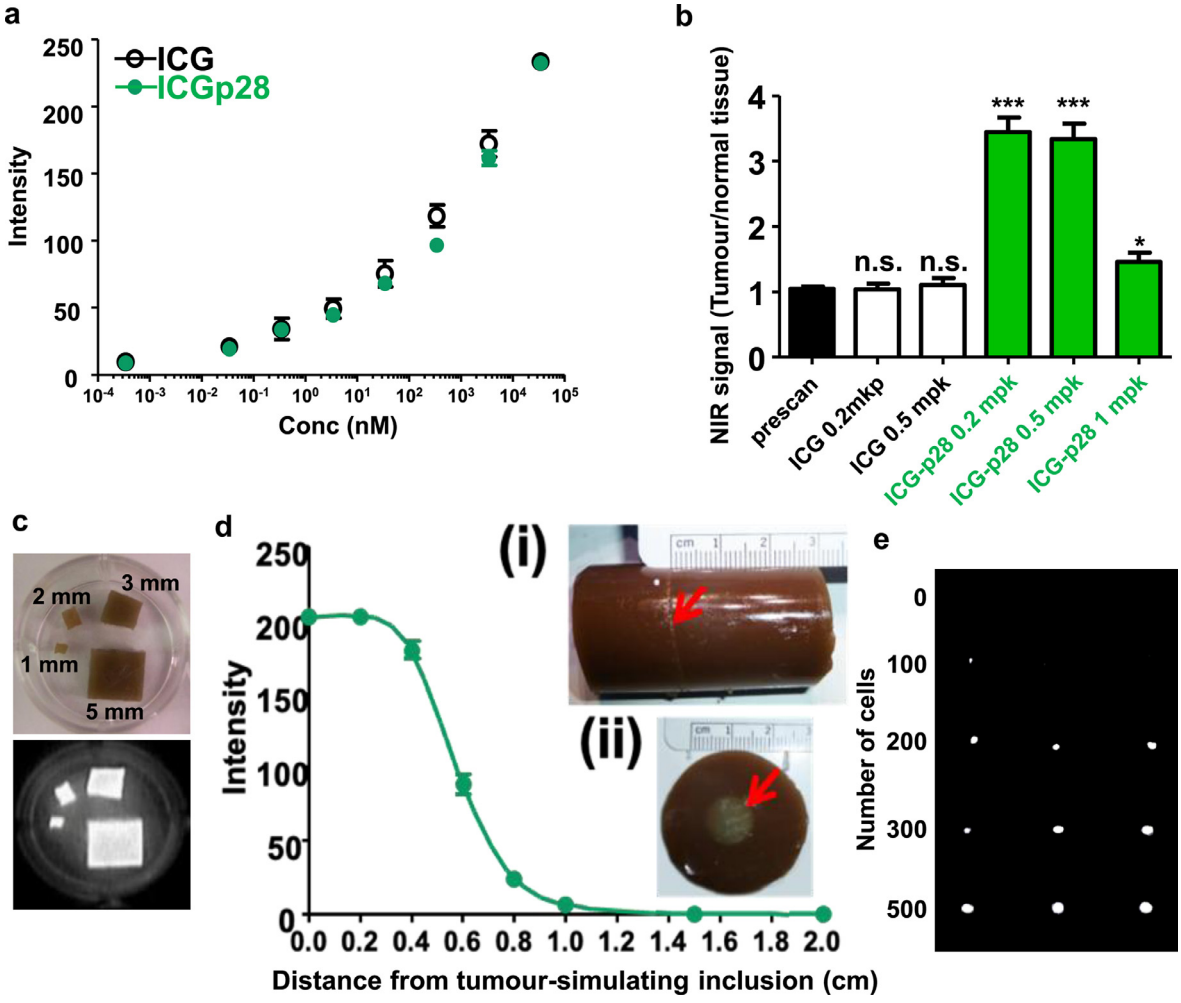

Figure 1. Characterization of ICG-p28. **a,** NIR fluorescence from ICG-p28 or ICG in a 5% intralipid emulsion was recorded with the PDE unit at 3 mW/cm^2 excitation intensity ($N = 3$). The intralipid solution alone showed no fluorescence and thus served as a control. The fluorescence quantum yield (ΦF) of ICG-p28 was similar to that of ICG at picomolar to micromolar concentrations. **b,** The signal-to-noise ratio (signal at 800 nm: tumour, noise: surrounding normal tissue, thigh muscles) in MDA-MB-231 tumour-bearing mice was recorded with the PDE unit and quantitatively analysed in a dose-dependent manner. The prescans were performed before injection of the NIR agent. ***: $P < 0.001$, *: $P < 0.05$ (ANOVA), n.s.: not significant mpk: mg/kg. **c,** The specific NIR signals (800 nm) of tumour-simulating inclusions of different sizes (1−3 and 5 mm) containing 200 nM ICG-p28 were measured. **d,** The specific NIR signals (800 nm) of tumour-simulating inclusions containing 200 nM ICG-p28 inserted into phantoms at depths of 0−2 cm were measured. **d(i),** Side view of the phantom. **d(ii)**, Top view of the phantom. Red arrows: locations of the tumour-simulating inclusions. The distance between the PDE camera (which captured images at 3 mW/cm^2 excitation intensity) and the phantom was fixed at 200 mm. The results are presented as the mean+SD. **e,** NIR fluorescence (800 nm) from various numbers of MDA-MB-231 cells ($N = 3$ in each cell number) exposed to ICG-p28 at 0.5 mg/kg for 2 h were recorded with the PDE unit.

the smallest objective (1 mm), NIR fluorescence imaging of ICG-p28 at nanomolar concentrations was able to detect NIR-specific signals (Figure 1c) and probe tissue at a depth of approximately one centimetre in an intralipid emulsion mimicking tissue scattering properties (Figure 1d). We also estimated the detection limit of the cell number *in vitro*. Cancer cell suspensions with various numbers of MDA-MB231 were imaged with the PDE unit. NIR-specific signals were detected from MDA-MB-231 cells as low as 200 cells in 1 mm size (Figures 1e, *Supplemental S2*).

Based on these imaging and dosing parameters, we performed real-time PDE imaging of immunodeficient mice with two different subtypes of human breast cancer: oestrogen receptor (ER)-positive breast cancer, which accounts for approximately 80% of all human breast cancers,[41] and triple-negative breast cancer (TNBC; negative for ER, progesterone, and Her2

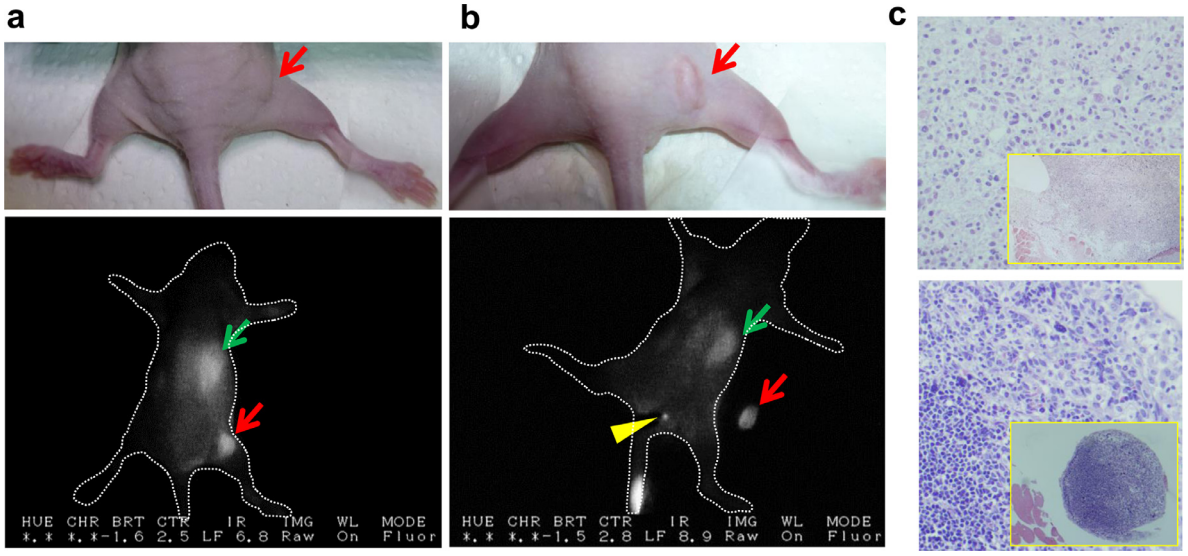

Figure 2. Real-time imaging with ICG-p28 in xenograft mouse models. MDA-MB-231 (**a**) or IOWA-1T (**b**) breast cancer cells were injected *s.c.* into mice ($N = 8$ in each cell line). Once the tumours (<10 mm) developed, 0.5 mg/kg ICG-p28 was injected *i.v.* into the mice. Twenty-four hours post-ICG-p28 injection, the mice were imaged with the PDE system during tumour removal. White light photographs (upper) and snapshot NIR PDE images are shown (lower; dorsal view, greyscale at 800 nm). The liver (green arrows) showed relatively high signal intensity from the excretion of ICG. Red arrows: tumours. The representative animal image showed the preferential uptake of ICG-p28 in a small lymph node (LN, yellow arrowhead in **b**). **c,** H&E-stained sections of the primary tumour (upper) and a sciatic LN (lower, yellow arrowhead) located at the superficial gluteal muscle, which was confirmed to be tumour positive (magnification 200x, inset 40x).

receptor expression), which accounts for 10–15% of all human breast cancers[42] and generally displays a poorer prognosis than ER-positive breast cancer. Athymic mice xenografted with MDA-MB-231 (TNBC) (Figure 2a) or IOWA-1T (ER+, PR-, Her2-) human breast cancer cells (Figure 2b) *s.c.* received a single injection of ICG-p28 *i.v.* at 0.5 mg/kg (~125 nmole/kg). Twenty-four hours after ICG-p28 injection, we observed the preferential uptake of ICG-p28 by tumours and clear contrast between the tumour and the surrounding tissue (Figure 2a,b), suggesting that our approach can be applied to broad types of breast cancer independent of receptor expression patterns. Notably, during tumour resection, intraoperative NIR imaging revealed the preferential uptake of ICG-p28 concentrated over a period of time in a small (≤1 mm) sciatic lymph node (LN) (Figure 2b). Hematoxylin and eosin (H&E)-stained sections confirmed the presence of cancer cells within the LN (Figure 2c), suggesting that ICG-p28 can identify other cancer foci in the breast parenchyma. Future studies are needed to explore the ability of ICG-p28 to identify positive lymph nodes during surgery.

ICG-p28-based assessment of the tumour margin in an MDA-MB-231-iRFP tumour-bearing model

To determine whether ICG-p28 can precisely delineate tumour margins, we created an MDA-MB-231-iRFP (TNBC) cell line that stably expresses the NIR fluorescence protein iRFP as a tumour marker. Although we do not intend to use the iRFP gene expression system in humans, it provides an excellent experimental model to assess the accuracy of tumour margin detection according to a real-time comparison of the fluorescence between iRFP and ICG-p28. The 700 nm channel is suitable for detecting tumours generated by these cells *in vivo*, as it can be used to monitor iRFP-specific fluorescence in cancer cells without affecting the 800 nm fluorescence and thus the signal from ICG-p28.[43,44] Confocal (Figure 3a) and LI-COR Odyssey (*Supplemental Figure S3*) images of MDA-MB-231-iRFP cells showed that the intracellular expression of the tumour marker iRFP allowed the accurate determination of tumour margins. ICG-p28 or ICG alone at 0.5 mg/kg was injected *i.v.* into athymic mice inoculated with MDA-MB-231-iRFP cells; 24 h later, the xenografted tumours and surrounding tissues were removed. The dotted lines in Figure 3b indicate the outer edges of the soft tissues. *Ex vivo* images showed good overlap between the NIR signals (merged) from iRFP (red: 700 nm) and ICG-p28 (green: 800 nm) (Figure 3b). Furthermore, similar to the results presented in Figs. 1 and 2, ICG alone exhibited poor tumour retention (Figure 3b). The concordance rates of 700 and 800 nm NIR signals in the ICG-p28 and ICG alone groups were 86% and 12%, respectively, (Figure 3c). These results indicate that

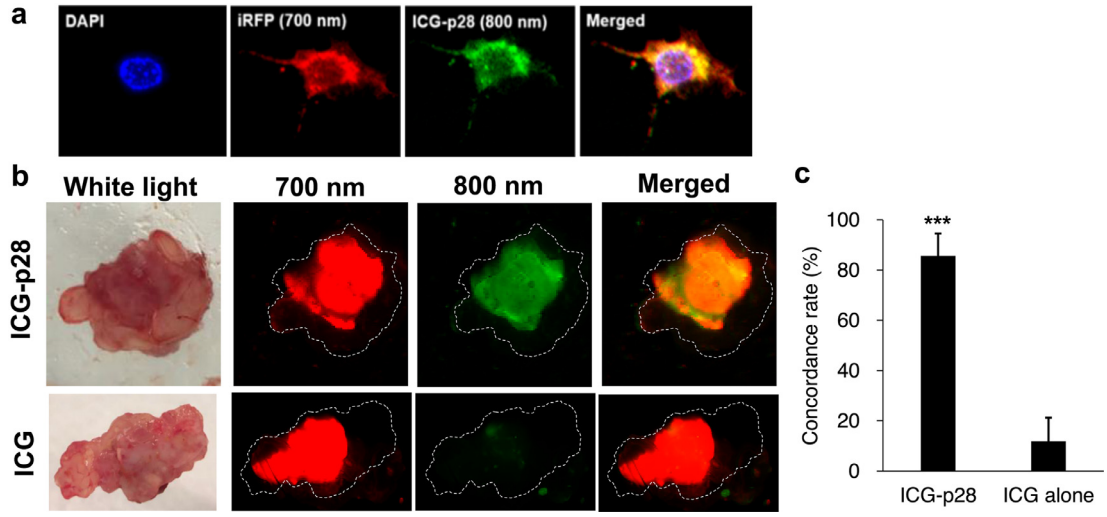

Figure 3. Colocalization of ICG-p28 and the tumour marker iRPF. **a,** ICG-p28-treated MDA-MB-231-iRFP cells were fixed in paraformaldehyde, and images were acquired under a confocal microscope. Red: tumour marker iRFP (700 nm); green: ICG-p28 (800 nm); blue: DAPI (nucleus); yellow: red+green. **b,** Athymic mice bearing MDA-MB-231-iRFP tumours were injected *i.v.* with either ICG-p28 or ICG alone at 0.5 mg/kg. Twenty-four hours after injection, representative *ex vivo* images of the tumour and surrounding soft tissues for the ICG-p28 group (top row) and the ICG alone group (bottom row) were taken with an Odyssey scanner. The dotted line in the images indicates the outer edge of the soft tissue. iRFP (red: 700 nm); ICG-p28 or ICG (green: 800 nm); and colocalization (yellow-orange). **c,** Concordance rate of the fluorescent signal in each group [the ICG-p28 group ($N = 10$) and the ICG alone group ($N = 5$)]; ***: $P < 0.001$ (*t*-test). The results are presented as the mean + SD.

ICG-p28 can preferentially localize at tumour sites and enhance the stability of ICG due to p28 conjugation.

Intraoperative imaging of orthotopic xenografts

To evaluate whether real-time image-guided surgery can reduce tumour recurrence, orthotopic MFP xenograft tumour models were used. Athymic mice bearing TNBC MDA-MB-231 or ER-positive IOWA-1T tumours were treated with PBS, ICG alone or ICG-p28 (0.5 mg/kg, *i.v.*), and NIR fluorescence was monitored with the PDE system during tumour resection surgery, in which tumours and surrounding tissues with a 2 mm safe margin were removed. During tumour removal, no apparent adverse events related to the administration of ICG or ICG-p28 were observed, and there were no other complications during the procedures. For the control mice treated with PBS, only palpation and direct visualization without fluorescence imaging were used for margin determination. After tumour resection, tumour recurrence resulting from remnant positive margins at the resection sites was evaluated (Figure 4a). Four weeks after tumour resection, recurrence was observed at the surgical sites in 31.2% (5/16) of mice in the PBS group and 25.0% (4/16) of mice in the ICG alone group. In sharp contrast, one of sixteen mice (6.3%) in the ICG-p28 group demonstrated tumour recurrence at the resection site. Representative images of the surgical sites in each group are shown (Figure 4b). The average volumes of the recurrent tumours were 944, 197, and 423 mm^3 in the PBS, ICG-p28, and ICG groups, respectively, (Figure 4c). Collectively, these findings show that by aiding in the precise identification of the tumour margins, ICG-p28 improved surgical outcomes by reducing both the incidence of tumour recurrence and the volume of recurring tumours.

Image-guided tumour resection in a PDX tumour model

PDX models are widely used in cancer research because of their distinct advantages in preserving the biological characteristics of the original human tumour.[45] Given the reduced tumour recurrence observed in the orthotopic xenograft models treated with ICG-p28-guided resection (Figure 4c), we utilized a PDX model[46,47] and a primary TNBC fragment (stage IV) to further evaluate ICG-p28 in a more clinically relevant model. In addition, to investigate whether this result was due to the specific motifs of p28, we included additional control peptides conjugated to ICG. Similar to p28, a noncationic CPP derived from annexins, named AA3H, was previously isolated and shown to penetrate cancer cells.[48] The other peptide was retro-inverso p28 (RI p28). RI modification is often used as an approach to generate a peptidomimetic, which represents the isomer of the parent peptide (p28) in which the direction of the sequence is reversed and the chirality of each amino acid residue is inverted.[49] Under anaesthesia, tumours and surrounding mammary tissues with a 2-mm safe margin were removed under real-time guidance with PDE imaging of mice injected with ICG-p28

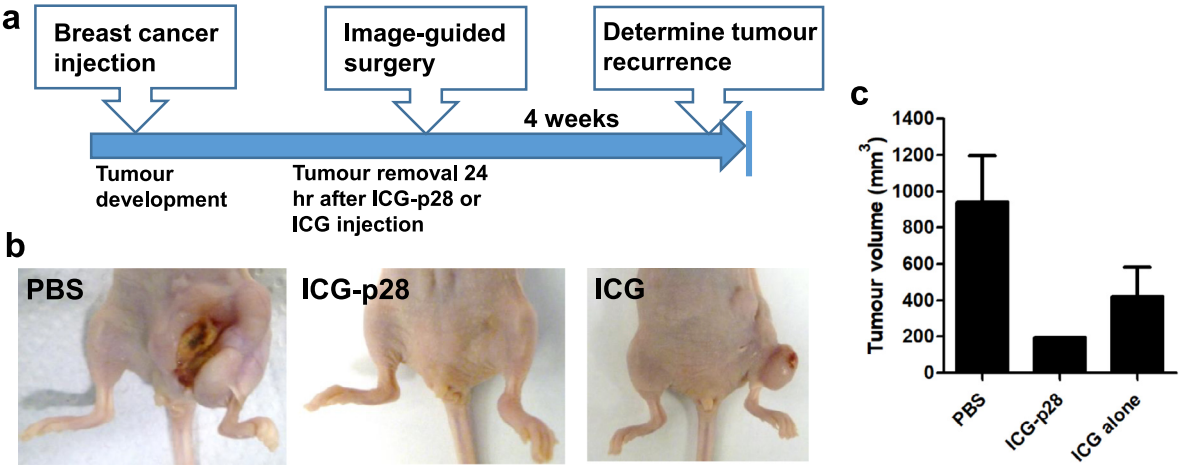

Figure 4. Intraoperative imaging of orthotopic xenograft models. **a,** A schematic diagram of the intraoperative imaging performed during tumour resection in human breast cancer xenograft tumour models. Human breast cancer cells (MDA-MB-231 or IOWA-1T) were inoculated into the fourth abdominal fat pad via *s.c.* injection at the base of the nipple. When the mice developed a tumour, they were injected with PBS, ICG-p28 or ICG at a concentration of 0.5 mg/kg. Twenty-four hours after injection, the tumours were resected while being visualized with the PDE imaging unit; the exception was the PBS group, whose tumours were identified only with palpation/direct visualization (no imaging guidance). After tumour resection, the mice were monitored for four additional weeks to detect any tumour recurrence. **c,** Representative images of tumour resection sites at the end of the study. **c,** Average volumes of the recurrent tumours (four weeks after tumour resection) in each group. The results are presented as the mean + SD.

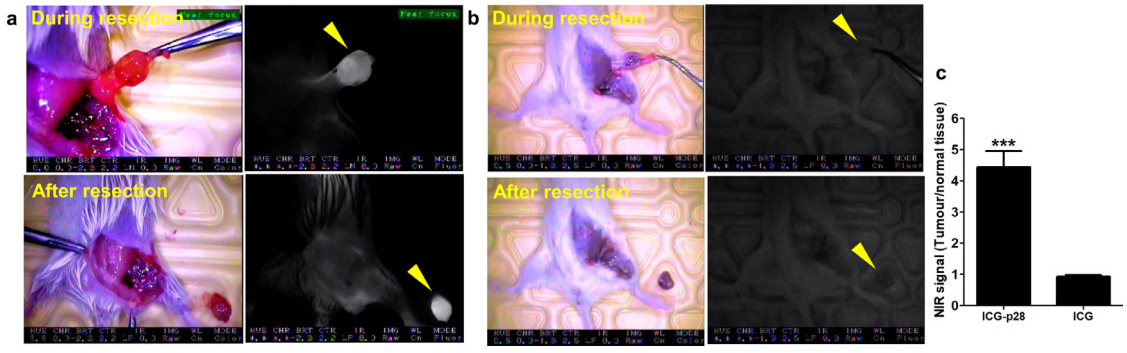

Figure 5. Image-guided surgery of human breast cancer PDX models. TNBC PDX cells were inoculated into the fourth abdominal fat pad. Twenty-four hours after NIR agent injection (**a,** ICG-p28, **b,** ICG alone), the tumours were resected under visualization with the PDE imaging unit. White light photographs (left) and snapshot NIR PDE images are shown (right; dorsal view, greyscale at 800 nm). Yellow arrowhead: tumour. **c,** The signal-to-noise ratio in PDX-bearing mice was recorded with the PDE unit and quantitatively analysed ($N = 8$ per group). ***: $P < 0.001$ (*t*-test). The results are presented as the mean+SD.

(Figure 5a), ICG alone (Figure 5b) or a control agent (PBS, ICG-RI-p28 or ICG-AA3H; *Supplemental Figure S4*). ICG-p28 provided significantly greater contrast enhancement and a more readily identified tumour than the control agents. These results show that the tumour-targeting ability of ICG-p28 is due to the specific motifs of p28.

Detection of residual cancer cells in the tumour margin by Alu sequencing

To quantitatively determine the efficacy of margin identification by our imaging approach, PCR-based assays were used to detect residual human cancer cells in the PDX models described above (Figure 5).[50] During image-guided surgery, tumours with a 2 mm safety margin and the surrounding mammary tissues at the 6 and 12 o'clock positions were removed in real time under guidance of the PDE imaging system (Figure 6a). These samples were collected to undergo huAlu PCR as well as traditional histological analyses. In the quantitative analysis using huAlu and the housekeeping gene mGAPDH, image-guided surgery with ICG-p28 showed significantly fewer residual cancer cells in the surrounding tissues [log(huAlu DNA/mGAPDH DNA) = -5.2] than surgery with the other agents [ICG

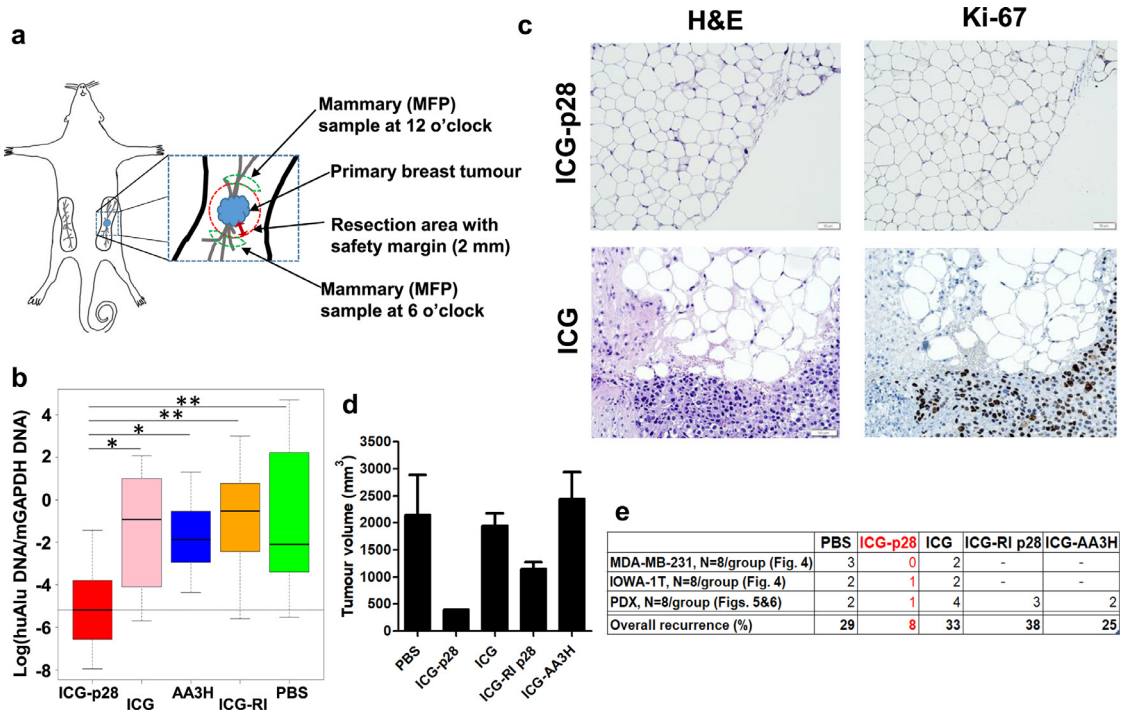

e

	PBS	ICG-p28	ICG	ICG-RI p28	ICG-AA3H
MDA-MB-231, N=8/group (Fig. 4)	3	0	2	-	-
IOWA-1T, N=8/group (Fig. 4)	2	1	2	-	-
PDX, N=8/group (Figs. 5&6)	2	1	4	3	2
Overall recurrence (%)	29	8	33	38	25

Figure 6. Detection of residual cancer cells in tumour margins. **a,** A schematic diagram of the sites of biopsy collection from NSG mice bearing PDX tumours (Mammary fat pad: MFP). **b,** Genomic DNA was extracted from each specimen and subjected to PCR assays. The box plot shows the values of log(huAlu DNA/mGAPDH DNA), calculated using standardized amounts of huAlu DNA and mGAPDH DNA among the agents. *: $P < 0.05$, **: $P < 0.005$ (F test). Results are presented as the mean ± SD. **c,** Histological analysis of surgical specimens. Representative images (200x) of H&E staining and staining for the proliferative marker Ki-67 to confirm the presence of negative margins in specimens obtained from the ICG-p28 group (top). The specimen obtained from the ICG group (bottom) shows the presence of malignant cells. **d,** Four weeks after surgical resection, the tumour volumes in each group were determined.

alone, ICG-AA3H, ICG-RI p28 or PBS: -0.9, -1.9, -0.5 and -2.1, respectively] (Figures 6b, *Supplemental S5)*. This finding indicated that image-guided surgery with ICG-p28 resulted in a 6.6 × 10^3-fold average reduction in residual normalized tumour DNA at the margin sites relative to surgery with the controls and that ICG-p28 precisely distinguished tumour margins better than the other agents. The coefficient of variation (CV) also indicated that ICG-p28 was superior to the other peptides/agents as an intraoperative probe, as it demonstrated a relatively small dispersion (*Supplemental Table S1*).

We next performed traditional histological analyses with H&E and proliferative marker Ki-67 staining on the set of tumour margin samples that were used for the Alu PCR assays. The results of these tests revealed that image-guided surgery with ICG-p28 could result in a clear negative margin at the edges of mammary tissues (Figure 6c). In the PDX tumour model, the positive margin rates of the PBS, ICG alone, ICG-RI p28 and ICG-AA3H groups were 19,19,31 and 38%, respectively, while malignant cell free margin (sixteen mammary tissue samples from eight mice) was obtained in the ICG-p28 group (Figures 6c, *Supplemental S6*). The histological data supported the results obtained from the Alu PCR assay, indicating that image-guided surgery with ICG-p28 improved the ability to precisely identify tumour margins.

As the tumour recurrence rate is a clinically significant indicator for positive margins, we determined the tumour recurrence rates in the PDX tumour model. Four weeks after image-guided surgery, the tumour recurrence rates for the surgical site were 25.0%, 50.0%, 12.5%, 37.5%, and 25.0% in the PBS, ICG alone, ICG-p28, ICG-RI p28 and ICG-AA3H groups, respectively. The average volumes of the recurrent tumours were 2151, 1952, 403, 1152, and 2447 mm^3 in the PBS, ICG alone, ICG-p28, ICG-RI p28, and ICG-AA3H groups, respectively, (Figure 6d). The average volumes of the recurrent tumours in the ICG-p28 group were the smallest among all groups tested. ICG-p28 provided greater contrast enhancement and a more readily identified tumour than the control agents (Figure 5c), which provided low contrast and made it difficult to remove the tumours completely. These findings suggest that image-guided surgery with ICG-p28 can precisely identify tumour margins, resulting in reduced tumour recurrence.

Discussion

In this study, ICG-p28, a new optical imaging probe, was characterized in terms of its photophysical properties, its specific uptake in tumours and its ability to precisely identify tumour margins in multiple human breast cancer mouse models. Intraoperative imaging with ICG-p28 was able to identify small (≤1 mm) LN metastases. Image-guided surgery with ICG-p28 improved positive margin identification and the tumour recurrence rate in multiple breast cancer animal models independent of the receptor expression status. In general, fluorescence imaging is a highly beneficial technique for the real-time assessment of tumour boundaries during surgical procedures and offers several advantages, such as the relatively low cost of the fluorescent dye and safety for the patient and the medical team, as non-invasive agents are used. Additionally, optical imaging with contrast enhancement can be used to visualize tumours prior to resection without changing the surgical field of view. Due to the preferential penetration of ICG-p28, substantial contrast between the tumour and surrounding normal tissues was achieved in multiple breast cancer animal models.

It has been reported that ICG alone at relatively high dose (5 mg/kg) can localize to the breast tumours, however it is likely that the lack of ligand specific binding allowed it to leak out of the tumour and easily infiltrate surrounding tissues over 24 h. A potential solution to overcome the limitations of ICG as a localizing contrast agent is to utilize a targeted NIR dye.[9] In contrast, timing of intraoperative imaging is a major concern when using 0.25 mg/kg of ICG alone for tumoural detection.[8] Similarly, the optimazation of such parameters for ICG-p28 has been done in this study. Higher doses of ICG-p28 (>1.0 mg/kg) required a longer time to obtain clear contrast because of the high background signal; thus, we found that the tumour-specific signal was optimal at an ICG-p28 concentration of 0.2−0.5 mg/kg within a time scale (24 h) practical for clinical use.[51] With the imaging and dosing parameters, ICG-p28 provided a significant contrast (TBR ~4-fold) in multiple breast cancer animal models. It is generally accepted that a TBR >3.0-fold is sufficient to provide adequate intraoperative contrast in studies on image-guided surgery and is essential for successful clinical translation.[52] In contrast, ICG alone was excreted rapidly, as expected, and the tumour site was not distinguishable (TBR ~1.1) under our experimental conditions. This observation also confirmed that the preferential uptake of the new compound was due to the presence of the p28 motif, which lead to longer retention at the tumour site and precise contrast imaging between the tumour and surrounding tissue. Although the molecular weight, pI, charge, hydrophobicity, and amino acid composition of RI p28 were exactly the same as those of p28, the overall entry of RI p28 was significantly decreased, and it did not show preferential entry (Figures 6, *Supplemental S4*). This finding suggests that the preferential entry of p28 is amino acid sequence-specific/stereochemically specific. Currently, various types of NIR imaging probes have been tested for different cancers, such as glioma and lung, pancreatic, colorectal, prostate, and breast cancers.[53] A series of investigational fluorescent agents, such as bevacizumab-IRDye800 (vascular endothelial growth factor A),[54] EC17 fluorescent dye (folate-receptor alpha),[55] the cathepsin activatable fluorescent agent LUM015 (a cathepsin protease),[56] and tozuleristide (a matrix metalloprotease),[57] are being validated for use in image-guided surgery. In comparison, the use of p28 has several advantages: **(i)** unlike use of antibodies,[37] the chemical conjugation of p28 to ICG does not alter ICG fluorescence (Figure 1a), **(ii)** p28 can target a wide range of breast cancers independent of the receptor status (Figures 2,5,6), **(iii)** ICG-p28 is composed of the clinically non-toxic tumour-targeting p28 peptide with the FDA-approved NIR ICG dye, and **iv)** our technique can be applied to other types of solid tumours as p28 preferentially enters various types of cancer cells.[19,58]

Image-guided surgery with ICG-p28 in the PDX model resulted in tumour recurrence in one of eight mice (Figure 6d). However, the Alu PCR assay and histological analyses did not reveal residual tumours in the MFP specimen obtained at either the 6 o'clock or the 12 o'clock position. There are two possible reasons for this phenotype. One possibility is that cancer cells were not captured by histological analyses. Although the specimen was determined to be tumour negative by histology and the Alu analyses, it may have contained a small number of tumour cells (probably <200 cells) that were otherwise missed, indicating a possible microinvasive breast tumour measuring less than 1 mm in size.[59] Lesions of this size would not be visible without a microscope and would have been left unresected in the tumour bed. If this is the case, additional approaches (e.g., image-guided surgery with ICG-p28 in combination with other therapeutic approaches) need to be further considered to manage these microlesions. The other possibility is that the precursor-like lesion (*e.g.*, atypical hyperplasia) which was captured in the histological section of the MFP specimen (*Supplemental Figure S7)* was left behind in the surgical bed. As PDX tumours can contain several precursor lesions such as atypical hyperplasia, flat epithelial atypia, pagetoid lobular carcinoma *in situ*,[60] it is possible that they can be a source of invasive/noninvasive breast cancer due to the characteristics of the PDX models.[61,62] Since we are aware that the complete surgical excision of the early stage of disease with negative margins is important from the clinical point of view, intraoperative imaging on the early stage of disease is currently under investigation. Nevertheless, given that only one mouse in the ICG-p28 group demonstrated tumour recurrence and that the volume of the

recurred tumour was the smallest among the other groups, ICG-p28-guided surgery appears to assist well in precisely identifying tumour margins and to significantly reduce tumour recurrence rates. Overall, image-guided surgery with ICG-p28 in multiple subtypes of breast cancer (Figures 4,6) resulted in an average recurrent tumour volume of 300 mm^3, whereas surgery with ICG alone or without interoperative imaging (PBS) resulted in average recurrent tumour volumes of 1188 mm^3 (P = 0.017, Friedman's test) and 1289 mm^3 (P = 0.032, Friedman's test), respectively. In addition, the tumour recurrence rate for the ICG-p28 groups was 8% (92% specificity, N = 2/24), while the tumour recurrence rates for the ICG and PBS groups were 33% (N = 8/24) and 29% (N = 7/24), respectively, (Figure 6e). These results in multiple breast cancer animal models suggest that ICG-p28 improved surgical outcomes by reducing both the incidence of tumour recurrence and the volume of recurrent tumours through clear margin identification. Thus, the versatility of ICG-p28 can potentially reduce the risks of recurrence and reoperation for a broad type of breast cancer independent of the receptor expression status, minimize damage to healthy tissues and healthcare costs, improve postoperative quality of life, and increase patient survival rates.

Many imaging modalities, such as MRI, X-ray, CT, PET and ultrasound, have considerable roles in preoperative staging and intraoperative planning, while fluorescence imaging can be used during intraoperative surgical inspection and practice due to its superior resolution and sensitivity.[63] The PDE imaging system is a clinical and portable fluorescence imaing unit with the advantages of lower cost and ease of operation.[64] It would be more useful if NIR fluorescence image can overlay on top of the color bright field image as it would provide clearer anatomical landmarks during surgery. The precise identification of tumour margins is the major objective for effective surgical treatment of breast cancer as well as many other types of solid tumours. Inadequate positive margin identification frequently occurs in ~5% of resections of lung and kidney tumours, in ~20% of resections of breast, prostate and rectal cancer and in up to 40–60% of resections of vulvar and oral cancer.[65] Although we focused on breast cancer in this study, p28 can also enter cells of other types of cancer[19]; therefore, we envisage that our imaging approach can also be applied in the treatment of other types of cancer. Our real-time intraoperative imaging approach has the potential to positively impact the surgical treatment outcomes (e.g., morbidity, quality of life and costs) of many types of solid tumours.

Declaration of interests

The authors declare no competing interests.

Contributors

Conceptualization and Design: MG, SN, KC, TKDG, TY. Data collection: MG, IR, SN, SM, KC, AG, AS, TY. Data Analysis: MG, SM, JW, TY. Writing draft and Editing: MG, SN, KC, JW, TKDG, TY. Verification of the underlying data: MG, TY. All authors reviewed, discussed, and agreed with manuscript.

Acknowledgments

piRFP plasmid was kindly gifted from Dr. Y. L. Tang (Vascular Biology center, Medical College of Georgia, Augusta University). This work was supported by NIH/National Institute of Biomedical Imaging and Bioengineering, R01EB023924 to TY. Parts of this work were presented at the 2020 AACR Annual Meeting (LB-022). This work made use of facilities in the BRL at UIC, Keck Biophysics Facility at Northwestern University, and Integrated Light Microscopy at University of Chicago.

Data sharing statement

The data supporting the findings of this study are available within the article and/or the supplementary materials. The data not shown can be available from the corresponding author upon reasonable requests.

Supplementary materials

Supplementary material associated with this article can be found in the online version at doi:10.1016/j.ebiom.2022.103850.

References

1 Siegel RL, Miller KD, Jemal A. Cancer statistics, 2020. *CA Cancer J Clin*. 2020;70(1):7–30.
2 McCahill LE, Single RM, Aiello Bowles EJ, et al. Variability in reexcision following breast conservation surgery. *Jama*. 2012;307(5):467–475.
3 Moran MS, Schnitt SJ, Giuliano AE, et al. Society of surgical oncology-american society for radiation oncology consensus guideline on margins for breast-conserving surgery with whole-breast irradiation in stages I and II invasive breast cancer. *J Clin Oncol*. 2014;32(14):1507–1515.
4 Vahrmeijer AL, Hutteman M, van der Vorst JR, van de Velde CJ, Frangioni JV. Image-guided cancer surgery using near-infrared fluorescence. *Nat Rev Clin Oncol*. 2013;10(9):507–518.
5 Gierach GL, Choudhury PP, García-Closas M. Toward risk-stratified breast cancer screening: considerations for changes in screening guidelines. *JAMA Oncol*. 2020;6(1):31–33.
6 Schwarz J, Schmidt H. Technology for intraoperative margin assessment in breast cancer. *Ann Surg Oncol*. 2020;27(7):2278–2287.
7 Hong G, Antaris AL, Dai H. Near-infrared fluorophores for biomedical imaging. *Nat Biomed Eng*. 2017;1(1):0010.
8 Pop FC, Veys I, Vankerckhove S, et al. Absence of residual fluorescence in the surgical bed at near-infrared fluorescence imaging predicts negative margins at final pathology in patients treated with breast-conserving surgery for breast cancer. *Eur J Surg Oncol*. 2021;47(2):269–275. The journal of the European Society of Surgical Oncology and the British Association of Surgical Oncology.

9 Keating J, Tchou J, Okusanya O, et al. Identification of breast cancer margins using intraoperative near-infrared imaging. *J Surg Oncol*. 2016;113(5):508–514.
10 Kedrzycki MS, Leiloglou M, Chalau V, et al. The impact of temporal variation in indocyanine green administration on tumor identification during fluorescence guided breast surgery. *Ann Surg Oncol*. 2021;28(10):5617–5625.
11 Xiao Q, Chen T, Chen S. Fluorescent contrast agents for tumor surgery. *Exp Ther Med*. 2018;16(3):1577–1585.
12 Sheng Z, Hu D, Xue M, He M, Gong P, Cai L. Indocyanine green nanoparticles for theranostic applications. *Nano-Micro Lett*. 2013;5(3):145–150.
13 Longo R, Torino F, Gasparini G. Targeted therapy of breast cancer. *Curr Pharm Des*. 2007;13(5):497–517.
14 Hernot S, van Manen L, Debie P, Mieog JSD, Vahrmeijer AL. Latest developments in molecular tracers for fluorescence image-guided cancer surgery. *Lancet Oncol*. 2019;20(7):e354–e67.
15 Madani F, Lindberg S, Langel U, Futaki S, Graslund A. Mechanisms of cellular uptake of cell-penetrating peptides. *J Biophys*. 2011;2011: 414729.
16 Vale N, Duarte D, Silva S, et al. Cell-penetrating peptides in oncologic pharmacotherapy: a review. *Pharmacol Res*. 2020;162: 105231.
17 Yamada T, Mehta RR, Lekmine F, et al. A peptide fragment of azurin induces a p53-mediated cell cycle arrest in human breast cancer cells. *Mol Cancer Ther*. 2009;8(10):2947–2958.
18 Taylor BN, Mehta RR, Yamada T, et al. Noncationic peptides obtained from azurin preferentially enter cancer cells. *Cancer Res*. 2009;69(2):537–546.
19 Yamada T, Signorelli S, Cannistraro S, Beattie CW, Bizzarri AR. Chirality switching within an anionic cell-penetrating peptide inhibits translocation without affecting preferential entry. *Mol Pharm*. 2015;12(1):140–149.
20 Razzak M. Targeted therapies: one step closer to drugging p53. *Nat Rev Clin Oncol*. 2013;10(5):246.
21 Warso MA, Richards JM, Mehta D, et al. A first-in-class, first-in-human, phase I trial of p28, a non-HDM2-mediated peptide inhibitor of p53 ubiquitination in patients with advanced solid tumours. *Br J Cancer*. 2013;108(5):1061–1070.
22 Lulla R, Goldman S, Beattie CW, et al. Phase 1 trial of p28 (NSC745104), a non-HDM2 mediated peptide inhibitor of p53 ubiquitination in children with recurrent or progressive CNS tumors: a final report from the Pediatric Brain Tumor Consortium. *Neuro Oncol*. 2016. https://doi.org/10.1093/neuonc/now047. First published online: March 28, 2016.
23 Jia L, Gorman GS, Coward LU, et al. Preclinical pharmacokinetics, metabolism, and toxicity of azurin-p28 (NSC745104) a peptide inhibitor of p53 ubiquitination. *Cancer Chemother Pharmacol*. 2011;68(2):513–524.
24 Singletary SE. Surgical margins in patients with early-stage breast cancer treated with breast conservation therapy. *Am J Surg*. 2002;184(5):383–393.
25 Young Kim H, Young Yum S, Jang G, Ahn DR. Discovery of a non-cationic cell penetrating peptide derived from membrane-interacting human proteins and its potential as a protein delivery carrier. *Sci Rep*. 2015;5:11719.
26 Naffouje S, Goto M, Ryoo I, Green A, Das Gupta TK, Yamada T. book chapter title: A method of tumor *in vivo* imaging with a new peptide-based fluorescent probe. Methods Mol Biol. 2021;2394. In press.
27 Abo T, Nanashima A, Tobinaga S, et al. Usefulness of intraoperative diagnosis of hepatic tumors located at the liver surface and hepatic segmental visualization using indocyanine green-photodynamic eye imaging. *Eur J Surg Oncol*. 2015;41(2):257–264.
28 Choukeife JE, L'Huillier JP. Measurements of scattering effects within tissue-like media at two wavelengths of 632.8 nm and 680 nm. *Lasers Med Sci*. 1999;14(4):286–296.
29 Pleijhuis RG, Langhout GC, Helfrich W, et al. Near-infrared fluorescence (NIRF) imaging in breast-conserving surgery: assessing intraoperative techniques in tissue-simulating breast phantoms. *Eur J Surg Oncol*. 2011;37(1):32–39.
30 Pleijhuis R, Timmermans A, De Jong J, De Boer E, Ntziachristos V, Van Dam G. Tissue-simulating phantoms for assessing potential near-infrared fluorescence imaging applications in breast cancer surgery. *J Vis Exp*. 2014:(91):51776.
31 Kim J, Yu W, Kovalski K, Ossowski L. Requirement for specific proteases in cancer cell intravasation as revealed by a novel semiquantitative PCR-based assay. *Cell*. 1998;94(3):353–362.
32 Nguyen QT, Olson ES, Aguilera TA, Jiang T, Scadeng M, Ellies LG, et al. Surgery with molecular fluorescence imaging using activatable cell-penetrating peptides decreases residual cancer and improves survival. *Proc Natl Acad Sci USA*. 2010;107(9):4317–4322.
33 Jing R, Zhou X, Zhao J, et al. Fluorescent peptide highlights micronodules in murine hepatocellular carcinoma models and humans *in vitro*. *Hepatology*. 2018;68(4):1391–1411.
34 Unno N, Suzuki M, Yamamoto N, et al. Indocyanine green fluorescence angiography for intraoperative assessment of blood flow: a feasibility study. *Eur J Vasc Endovasc Surg*. 2008;35(2):205–207.
35 Reinhart MB, Huntington CR, Blair LJ, Heniford BT, Augenstein VA. Indocyanine green: historical context, current applications, and future considerations. *Surg Innov*. 2016;23(2):166–175.
36 Ahmed MA, Aleskandarany MA, Rakha EA, et al. A CD44(-)/CD24(+) phenotype is a poor prognostic marker in early invasive breast cancer. *Breast Cancer Res Treat*. 2012;133(3):979–995.
37 Ogawa M, Kosaka N, Choyke PL, Kobayashi H. *In vivo* molecular imaging of cancer with a quenching near-infrared fluorescent probe using conjugates of monoclonal antibodies and indocyanine green. *Cancer Res*. 2009;69(4):1268–1272.
38 Vahrmeijer AL, Hutteman M, van der Vorst JR, van de Velde CJ, Frangioni JV. Image-guided cancer surgery using near-infrared fluorescence. *Nat Rev Clin Oncol*. 2013;10(9):507–518.
39 Hyun H, Park MH, Owens EA, et al. Structure-inherent targeting of near-infrared fluorophores for parathyroid and thyroid gland imaging. *Nat Med*. 2015;21(2):192–197.
40 Schwarz RA, Gao W, Redden Weber C, et al. Noninvasive evaluation of oral lesions using depth-sensitive optical spectroscopy. *Cancer*. 2009;115(8):1669–1679.
41 Pham TH, Page YL, Percevault F, Ferrière F, Flouriot G, Pakdel F. Apigenin, a partial antagonist of the estrogen receptor (ER), inhibits er-positive breast cancer cell proliferation through Akt/FOXM1 signaling. *Int J Mol Sci*. 2021;22(1):470.
42 Lu H, Samanta D, Xiang L, et al. Chemotherapy triggers HIF-1-dependent glutathione synthesis and copper chelation that induces the breast cancer stem cell phenotype. *Proc Natl Acad Sci USA*. 2015;112(33):E4600–E4609.
43 Hock AK, Lee P, Maddocks OD, Mason SM, Blyth K, Vousden KH. iRFP is a sensitive marker for cell number and tumor growth in high-throughput systems. *Cell Cycle*. 2014;13(2):220–226.
44 Jiguet-Jiglaire C, Cayol M, Mathieu S, et al. Noninvasive near-infrared fluorescent protein-based imaging of tumor progression and metastases in deep organs and intraosseous tissues. *J Biomed Opt*. 2014;19(1):16019.
45 Hidalgo M, Amant F, Biankin AV, et al. Patient-derived xenograft models: an emerging platform for translational cancer research. *Cancer discov*. 2014;4(9):998–1013.
46 DeRose YS, Gligorich KM, Wang G, et al. *Patient-Derived Models of Human Breast Cancer: Protocols for* In Vitro *and* In Vivo *Applications in Tumor Biology and Translational Medicine*. *Current Protocols in Pharmacology*. John Wiley & Sons, Inc.; 2001.
47 Hanna C, Kwok L, Finlay-Schultz J, Sartorius CA, Cittelly DM. Labeling of breast cancer patient-derived xenografts with traceable reporters for tumor growth and metastasis studies. *J Vis Exp*. 2016;117:54944.
48 Pavlova I, Williams M, El-Naggar A, Richards-Kortum R, Gillenwater A. Understanding the biological basis of autofluorescence imaging for oral cancer detection: high-resolution fluorescence microscopy in viable tissue. *Clin Cancer Res*. 2008;14(8):2396–2404. An official journal of the American Association for Cancer Research.
49 Taylor EM, Otero DA, Banks WA, O'Brien JS. Retro-inverso prosaptide peptides retain bioactivity, are stable *in vivo*, and are blood-brain barrier permeable. *J Pharmacol Exp Ther*. 2000;295(1):190–194.
50 Schneider T, Osl F, Friess T, Stockinger H, Scheuer WV. Quantification of human Alu sequences by real-time PCR—an improved method to measure therapeutic efficacy of anti-metastatic drugs in human xenotransplants. *Clin Exp Metastasis*. 2002;19(7):571–582.
51 Dalerba P, Cho RW, Clarke MF. Cancer stem cells: models and concepts. *Annu Rev Med*. 2007;58:267–284.
52 Tummers WS, Warram JM, van den Berg NS, et al. Recommendations for reporting on emerging optical imaging agents to promote clinical approval. *Theranostics*. 2018;8(19):5336–5347.
53 Jiao J, Zhang J, Yang F, et al. Quicker, deeper and stronger imaging: a review of tumor-targeted, near-infrared fluorescent dyes for fluorescence guided surgery in the preclinical and clinical stages.

Eur J Pharm Biopharm. 2020;152:123–143. official journal of Arbeitsgemeinschaft fur Pharmazeutische Verfahrenstechnik eV.
54 Lamberts LE, Koch M, de Jong JS, et al. Tumor-specific uptake of fluorescent bevacizumab-IRDye800CW microdosing in patients with primary breast cancer: a phase I feasibility study. *Clin Cancer Res*. 2017;23(11):2730–2741.
55 Tummers QR, Hoogstins CE, Gaarenstroom KN, et al. Intraoperative imaging of folate receptor alpha positive ovarian and breast cancer using the tumor specific agent EC17. *Oncotarget*. 2016;7(22):32144–32155.
56 Blau R, Epshtein Y, Pisarevsky E, et al. Image-guided surgery using near-infrared Turn-ON fluorescent nanoprobes for precise detection of tumor margins. *Theranostics*. 2018;8(13):3437–3460.
57 Dintzis SM, Hansen S, Harrington KM, et al. Real-time visualization of breast carcinoma in pathology specimens from patients receiving fluorescent tumor-marking agent tozuleristide. *Arch Pathol Lab Med*. 2019;143(9):1076–1083.
58 Taylor BN, Mehta RR, Yamada T, et al. Noncationic peptides obtained from azurin preferentially enter cancer cells. *Cancer Res*. 2009;69(2):537–546.
59 Giuliano AE, Connolly JL, Edge SB, et al. Breast cancer-major changes in the american joint committee on cancer eighth edition cancer staging manual. *CA Cancer J Clin*. 2017;67(4):290–303.
60 Fiche M, Scabia V, Aouad P, et al. Intraductal patient-derived xenografts of estrogen receptor α-positive breast cancer recapitulate the histopathological spectrum and metastatic potential of human lesions. *J Pathol*. 2019;247(3):287–292.
61 Santner SJ, Dawson PJ, Tait L, et al. Malignant MCF10CA1 cell lines derived from premalignant human breast epithelial MCF10AT cells. *Breast Cancer Res Treat*. 2001;65(2):101–110.
62 Dobrolecki LE, Airhart SD, Alferez DG, et al. Patient-derived xenograft (PDX) models in basic and translational breast cancer research. *Cancer Metastasis Rev*. 2016;35(4):547–573.
63 Wang P, Fan Y, Lu L, et al. NIR-II nanoprobes *in-vivo* assembly to improve image-guided surgery for metastatic ovarian cancer. *Nat Commun*. 2018;9(1):2898.
64 McGregor A, Pavri SN, Tsay C, Kim S, Narayan D. Use of indocyanine green for sentinel lymph node biopsy: case series and methods comparison. *Plast Reconstr Surg Glob Open*. 2017;5(11):e1566. [Internet]2017/11//.
65 Heidkamp J, Scholte M, Rosman C, Manohar S, Fütterer JJ, Rovers MM. Novel imaging techniques for intraoperative margin assessment in surgical oncology: a systematic review. *Int J Cancer*. 2021;149(3):635–645.